

Towards Mirror-Less Graphene-Based Perfect Absorbers

Sangjun Lee and Sangin Kim * 

Department of Electrical and Computer Engineering, Ajou University, Suwon 16499, Republic of Korea; lsjkmjh@ajou.ac.kr

* Correspondence: sangin@ajou.ac.kr

Abstract: Owing to its exceptional electronic and optical properties, graphene has attracted extensive attention among researchers in the development of high-performance optoelectronic devices. However, the light absorption of pure graphene is very poor, limiting its development in practical application. In this review, as a solution for this issue, various types of graphene-based perfect absorbers are addressed in terms of their operation principles and design requirements. Their recent progress and potential applications such as photodetectors and modulators are also discussed. In particular, we emphasize the importance of mirror-less (in particular, one-port mimicking) perfect absorber design due to simplified fabrication processes or enhanced tolerance for fabrication error.

Keywords: perfect absorption; graphene; tunable absorption; mirror-less

1. Introduction

Enhancing the light–matter interaction of various materials is of great importance in many optoelectronic device applications. A perfect absorber (PA) is a device in which the incident light wave at operating wavelengths can be perfectly absorbed via efficient light–matter interaction and then transformed into ohmic heat or other forms of energy [1–10]. It is not so difficult for thick absorbing materials to achieve highly enhanced absorption because the optical path length is proportional to thickness of absorbing medium. However, in ultrathin absorbing materials such as two-dimensional (2D) materials with atomic-layer thickness, high absorption cannot be obtained without proper engineering of the geometry of the structured elements. For example, pure monolayer graphene (with an atomically ultrathin thickness of ~0.34 nm), which is basically a semimetal with linear dispersion of two-dimensional Dirac fermions, has an optical absorption of ~2.3% under normal incidence in the near-IR to visible regime [6–11]. Here, pure graphene means that it is intrinsic or undoped. In addition, it does not include impurities such as oxygen, and it has a flat surface without any patterns. Thus, despite of its excellent carrier mobility, the weak light–matter interaction with graphene limits its development towards practical applications such as high-efficiency photodetection and modulation [12–16].

Here, we will address graphene perfect absorbers (GPAs). Over the past decade, to construct GPAs, various configurations have been proposed, such as asymmetric cavities using multiple layers [16–20], gratings or photonic crystals [21–33], metamaterials [34–40], and prism couplers [41–44]. Previous reviews on GPAs have mainly focused on categorization in terms of absorption bandwidth (for example, narrowband, dual-band, broadband) or their operating wavelength ranges (for example, Visible to THz band) [7–10]. In this topical review, these GPAs are classified into two types according to the presence or absence of 100% reflective external mirrors. As a typical external mirror, metal reflectors inevitably induce ohmic loss, and the distributed Bragg reflector (DBR) requires a sophisticated growth technique limited to certain material systems or the use of a complicated fabrication process, which are undesirable in applications such as modulators and photodetectors [14–16]. For example, in the asymmetric Fabry–Perot microcavity described in ref. [16] (which will also be addressed in the applications section), the bottom DBR,



Citation: Lee, S.; Kim, S. Towards Mirror-Less Graphene-Based Perfect Absorbers. *Appl. Sci.* **2023**, *13*, 9708. <https://doi.org/10.3390/app13179708>

Academic Editor: Philippe Lambin

Received: 19 July 2023

Revised: 14 August 2023

Accepted: 18 August 2023

Published: 28 August 2023



Copyright: © 2023 by the authors. Licensee MDPI, Basel, Switzerland. This article is an open access article distributed under the terms and conditions of the Creative Commons Attribution (CC BY) license (<https://creativecommons.org/licenses/by/4.0/>).

consisting of 25 pairs of alternating AIAs and AlGaAs layers, can be grown via molecular beam epitaxy (MBE) on an n-doped GaAs substrate. Owing to the low difference between the refractive indexes of AIAs and AlGaAs, the use of so many deposition processes is inevitable. Compared to conventional GPAs utilizing these external mirrors [14–44], mirrorless GPAs are desirable due to their simpler fabrication process, although their somewhat strict design requirements are inevitable [45–49]. In the case of the former, substantial progress has been made with respect to their development, but for the latter, development remains immature. We review the basic theory behind the two main types of GPAs in Sections 2 and 3, and then we discuss the performance of relevant potential applications in Section 4. Finally, the conclusions and future perspectives are provided in Section 5.

2. Graphene Perfect Absorbers with External Mirror

Before we get started the main issue, the optical properties of graphene need to be addressed. In the mid-IR to THz regime (strictly, $hf < 2E_f$, where h , f , and E_f are the Planck constant, the frequency of incident light, and the Fermi level of graphene, respectively), the optical conductivity of graphene is dominated by the intraband transition, and thus, it can be treated as a metallic material [6–10]. This indicates that doped graphene supports plasmon resonances, which are collective oscillations of free electrons. Unlike noble metals, free carriers in doped graphene can easily be tuned by electrostatic gating or chemical doping. Additionally, graphene plasmons have lower loss and stronger field confinement compared to plasmons in noble metals in the mid-IR to THz regime [7]. On the other hand, in the near-IR to visible regime (strictly, $hf > 2E_f$), absorption is nearly wavelength independent because its optical conductivity is dominated by the interband transition [6–10]. In particular, undoped monolayer graphene is treated as a lossy dielectric material that has an absorption efficiency of ~2.3% over a wideband wavelength range.

Under single-sided illumination, the most straightforward approach for achieving perfect absorption is to use a one-port resonant system that has a 100% reflective external mirror on the backside, as shown in Figure 1. In general, DBRs (distributed Bragg reflectors) and noble metals can be used as typical external mirrors for achieving zero transmission. According to the coupled mode theory (CMT), absorption efficiency in a lossy one-port resonant system can be described using the following equation [24,33,49]

$$A(\omega) = \frac{4\gamma_{leak}\gamma_{loss}}{(\omega - \omega_0)^2 + (\gamma_{leak} + \gamma_{loss})^2} \quad (1)$$

where ω_0 , γ_{leak} , and γ_{loss} are the resonant frequency, leakage rate, and loss rate, respectively. When $\gamma_{leak} = \gamma_{loss}$, $A = 1$ at resonance ($\omega = \omega_0$). This means that perfect absorption is achieved by balancing the internal loss rate and the external leakage (or coupling) rate of the resonator, commonly referred to as the ‘critical coupling’ condition. While γ_{leak} is controlled by the quality factor (Q-factor) of the resonator, γ_{loss} is controlled by the absorption coefficient and the electric field intensity in the graphene layer. The graphene absorption coefficient is determined by the doping level and the quality of the graphene, which can be generally described by the Kubo formula [6–10]. In this review, we mainly consider a CVD-grown graphene because it has moderate carrier mobility [50,51].

Due to the straightforward critical coupling concept, most previous perfect absorbers, including GPAs, have employed an external mirror [1–10]. When these GPAs support only single-resonance at wavelength range of interest, as shown in Figure 1 or Equation (1), they are dubbed as the ‘single-resonance/mirror absorber’. In the case of dual-band [52–56] or multi-band [57–62] absorption, the absorption efficiency can be described through the superposition of absorption in single-resonance/mirror absorbers with different resonances. In particular, ultra-broadband absorption [63–78] can be attributed to the overlapping of multiple resonance absorption bands which exhibit a significantly wider bandwidth. An alternative approach for implementing a one-port resonant system is ‘Prism-coupling absorber’ scheme [41–44], which utilizes total internal reflection (TIR) to achieve zero transmission. This implies that the prism functions as an external mirror at above critical

incident angles. While the prism-coupling scheme can provide a wide absorption bandwidth owing to its relatively weak resonance feature, its drawback is that it works only for an oblique incidence angle and has a bulky absorber system due to introduction of prism.

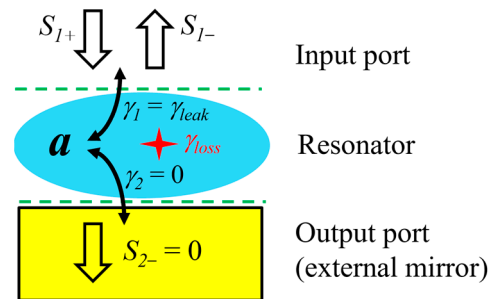


Figure 1. Schematic of a lossy one-port resonant system with an external mirror on the backside (that is, output port). a denotes the mode amplitude of the resonator. S_{1+} , S_{1-} , and S_{2-} are the incident, reflected, and transmitted field amplitudes, respectively. γ_1 ($=\gamma_{leak}$) and γ_2 ($=0$) denote the mode leakage rate to the front side and back side of the resonator, respectively. γ_{loss} denotes the loss rate of the resonator. The green dashed lines are reference planes for the field amplitudes in the ports.

2.1. 'Single-Resonance/Mirror Absorber' Scheme

As previously mentioned, perfect absorption in this absorption scheme can be attained when critical coupling condition is satisfied at resonance wavelength. Key parameters in Equation (1) (that is, leakage rate, loss rate, and resonance wavelength) are controlled by incident angle [18,19,41–44] or periodically patterned structures [21–40], as well as graphene doping level.

2.1.1. Absorption Control by Oblique Incidence

In 2017, Fan et al. [18] experimentally showed angle-selective giant light absorption by placing large-area unpatterned graphene on a structure consisting of a dielectric layer atop a gold mirror (Figure 2a). The doped graphene has metallic property due to $hf < 2E_f$. Such a simple structure supports a resonance mode with light trapped in the dielectric layer owing to the reflections at its top and bottom surfaces. The loss rate is insensitive to incident angle, whereas the leakage rate reaches zero at 90 degrees. Thus, the critical coupling condition can be always satisfied by adjusting the incident angle, even though the critical angle is a considerably high value. In ref. [19], the proposed structure can lead to perfect THz absorption because of strong light localization in the defect layer of the heterostructure using two Si/SiO₂ DBR (Figure 2b). When the incident angle increases, the resonant peak shifts toward higher frequencies due to the correlation between the resonance frequency and the incident angle. In 2016, Zhao et al. [20] proposed a multi-layer photonic configuration, which consists of an ultrathin metal film coated on a DBR and a graphene sheet in a silica spacer. The monolayer graphene exhibits an impressive absolute absorption of light, which can reach up to 80% (34.8-fold enhancement compared to the intrinsic value of 2.3%), due to the strong field confinement of Tamm plasmon in the silica spacer. The Tamm plasmon originates from the appropriate combination of a metal film (not a dielectric graphene) and a DBR. Changing the incident angle is a straightforward method to efficiently adjust the operating wavelength of graphene absorption. In detail, the absorption peak wavelength experiences a blueshift as the incident angle increases.

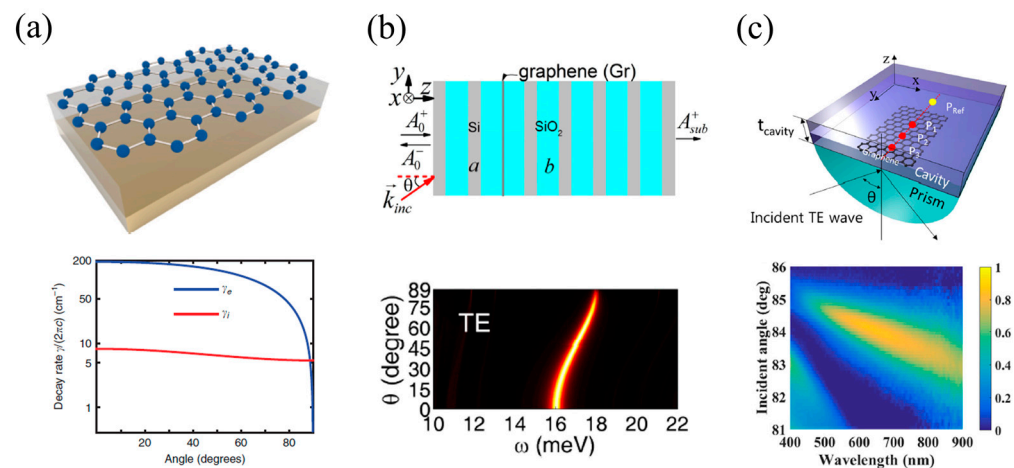


Figure 2. GPAs with angle-selective absorption. (a) Top: Schematic of a GPA consisting of monolayer graphene, separated from a gold mirror (light gray) by a dielectric spacer layer (dark gray). Bottom: leakage rate (blue line) and loss rate (red line) as a function of incident angle [18]. (b) Top: schematic of a GPA based on the strong light localization in the defect layer of heterostructure. Bottom: absorption spectra as a function of incident angle [19]. (c) Top: schematic of a GPA based on prism coupling, where monolayer graphene is embedded in the middle of dielectric cavity and a substrate is replaced with air. Bottom: measured absorption spectra by fundamental mode as a function of incident angle [43]. Reproduced with permission from [18,19,43], © 2023 Springer Nature; © 2023 Optical Society of America; © 2023 Elsevier Ltd.

In 2013, Pirruccio et al. [41] proposed a prism-coupling absorber in which a gap layer of an intermediate index value was embedded, and graphene was located at the interface between the gap layer and the substrate. They demonstrated broadband enhanced absorption with practically available materials by using five or ten layers of graphene. However, it is difficult to achieve perfect absorption for monolayer graphene due to the limitation on material index choice. In 2017, Kim et al. [42] proposed a modified absorber structure in which monolayer graphene is embedded in the middle of the gap layer, enabling practical perfect absorption in monolayer graphene with naturally available materials. The perfect absorption is attributed to enhanced light–graphene interaction through the creation of a cavity mode within the gap layer when a proper gap thickness and a graphene position are chosen. In 2019, the excellent performance of the proposed absorber was also experimentally demonstrated [43] (Figure 2c). The absorption peak is enhanced up to ~86% at $\lambda = 650$ nm with bandwidth of 314 nm (from 542 nm to 856 nm); this absorption performance is the best experimental result for monolayer graphene in the visible range, to the best of our knowledge.

2.1.2. Absorption Control by Patterned Structures

In the mid-IR to THz regime (strictly, $hf < 2E_f$), due to the metallic property of doped graphene, tunable graphene plasmons can be utilized by periodically patterning graphene itself. In 2012, Abajo et al. [21] reported that 100% light absorption can take place in the graphene disk arrays supported on a dielectric-coated gold surface, provided that the critical coupling condition is satisfied by properly choosing the dielectric coating layer thickness. Liu et al. [22] incorporated an air nano-slit into a similar structure, positioned at a specific displacement distance from its center, as illustrated in Figure 3a. The air nano-slit can not only exhibit an efficient asymmetrical characteristic for the graphene disk but also proposes a viable approach for realizing a high-Q resonant spectrum. Also, there have been many reports based on different metamaterials, such as graphene ribbon arrays [34,35], square metal patches [36], cross-shaped resonators [36,37], and split-ring resonators [36,38], as shown in Figure 3b–d. Most importantly, plasmon resonances in patterned graphene also

exhibit good absorption stability over a wide-angle range [34,35], as shown in Figure 3b, similarly to plasmon resonance in noble metals [31].

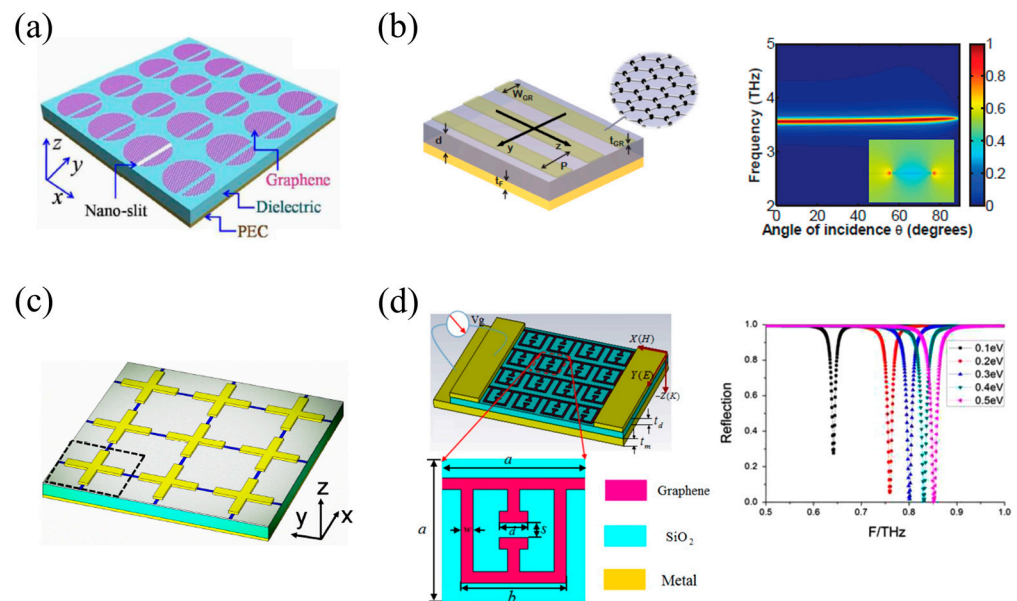


Figure 3. GPAs using periodically patterned metallic graphene. (a) Schematic of a GPA based on graphene disk array with air nano-slit [22]. (b) Left: schematic of a GPA based on graphene micro-ribbon. Right: absorption as a function of incident angle with dielectric thickness $d = 4.7$ mm for the first mode. Inset: electric field distribution E_y for the corresponding mode [34]. (c) Schematic of a GPA based on cross-shaped graphene [37]. (d) Left: schematic of a GPA based on graphene split-ring resonator and close-up view of unit cell. Right: reflection spectra for different Fermi levels [38]. Reproduced with permission from [22,34,37,38], © 2023 Elsevier Ltd.; 2012 Optical Society of America; 2014 Optical Society of America; © 2023 Elsevier B.V.

In near-IR to visible regime (strictly, $hf > 2E_f$), there is no plasmonic response in undoped graphene, so the critical coupling is entirely controlled by the resonance properties of the patterned structures excluding the graphene layer. To greatly enhance graphene absorption, a quite low γ_{leak} resonant structure is required to be balanced with quite low γ_{loss} . In many reports, unpatterned graphene is coupled with periodically patterned dielectric resonant structures of a high-Q. Fan et al. [24] and Qin et al. [25] numerically demonstrated that by using guided resonance in a photonic crystal slab backed by a DBR or a metal reflector, the absorption of monolayer graphene located on the top of a photonic crystal slab can reach perfect absorption (Figure 4a). By properly adjusting structural parameters such as period, thickness, and hole radius of photonic crystal slab, the system is critically coupled ($\gamma_{leak} = \gamma_{loss}$). Valentine et al. [26] and Zhou et al. [27] demonstrated experimentally close to total absorption in monolayer graphene absorbers based on critical coupling with guided resonances in transfer printed photonic crystal Fano resonance filters at near-IR.

In 2018, Lin et al. [39] introduced an asymmetric metasurface for an ultra-narrowband GPA. In the proposed absorber, in which monolayer graphene is on top of the dielectric metasurface backed by a silver substrate, the high angle tolerance and Q (~2600) are due to the magnetic dipole resonance based on two asymmetric silicon rings placed over a silica slab. Qin et al. [29] reported that peak absorptions over 99% with FWHM about 20 nm in the near-IR were measured for monolayer graphene coupled with subwavelength gratings on top of a back gold mirror (Figure 4b). The absorption structures shown are highly compact with a total thickness of less than $1\mu\text{m}$. In 2019, Kim et al. [33] proposed the narrowband GPAs with an exceptional fabrication tolerance, which consists of a low-contrast grating (LCG) and a finite DBR layer with monolayer graphene (Figure 4c). It is numerically

shown that the proposed GPA outperforms the previously proposed schemes in terms of fabrication tolerance. In addition, without degrading the fabrication tolerance, the bandwidth of the proposed absorber can be controlled by the DBR thickness (the number of pairs). For example, by stacking 8.5 Si/SiO₂ pairs in the DBR, a narrow absorption bandwidth of sub-nanometer can be attained.

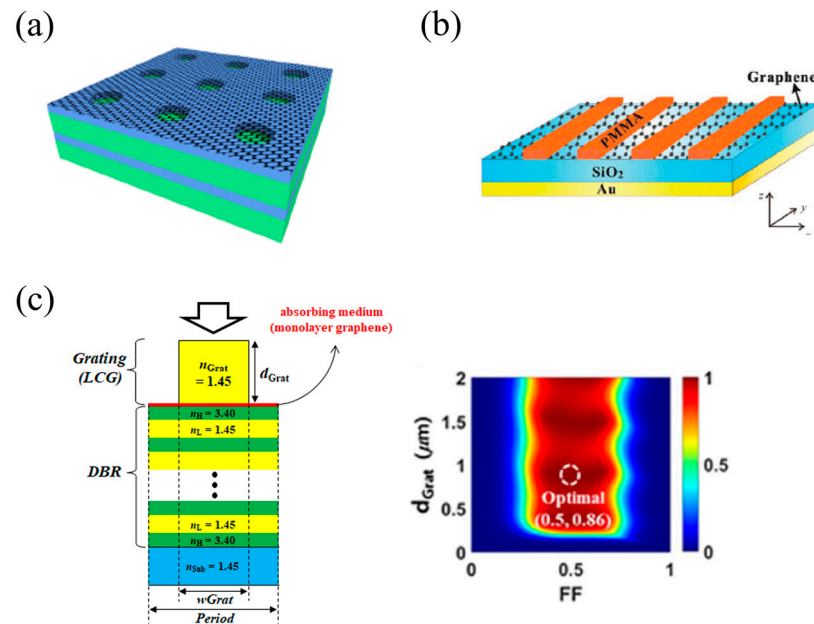


Figure 4. GPAs using unpatterned graphene and periodically patterned dielectric structures. (a) Schematics of a GPAs based on photonic crystal slab backed by DBR [24]. (b) Schematics of a GPAs based on PMMA grating on top of back gold mirror [29]. (c) Left: schematic of a GPA based on low-contrast grating (LCG) and DBR. Right: absorption map as a function of FF and d_{Grat} at $\lambda = 1550$ nm [33]. Reproduced with permission from [24,29,33], © 2023 American Chemical Society; © 2023 WILEY-VCH; © 2023 Springer Nature.

2.2. Performance Improvement of Absorbers

2.2.1. Angle-Insensitive Absorption

For certain graphene-based optoelectronic devices, achieving broadband graphene absorption with incident angle independence is highly desirable. In particular, GPAs designed by coupling the graphene with metal nanocavity can effectively provide angle-insensitive absorption due to the magnetic dipole resonance based on plasmon in metals [23,31]. In 2015, Kim et al. [23] proposed an electrically tunable absorber based on epsilon-near-zero (ENZ) effect of graphene embedded in a nanocavity, which is composed of metal grating and metal reflector (Figure 5a). When hf is close to $2E_f$, graphene can be an ENZ material with vanishingly small permittivity [23,79] at certain wavelengths under the proper contributions of interband and intraband transitions. Due to the strong surface-normal electric field confined in ENZ graphene, greatly enhanced absorption is achieved. Moreover, owing to the ENZ effect and the magnetic dipole resonance, it has a unique feature of incident angle insensitiveness. In 2018, Qin et al. [31] also demonstrated the GPA based on a deep subwavelength 2D square plate, where graphene has a dielectric property because undoped graphene is applied (Figure 5b). Similarly to the structure described in ref. [23], the electric field is mostly concentrated around the bottom corners of the silver plates, and the magnetic field is highly confined in the dielectric layer between the silver plates and silver reflection mirror. The direction of the magnetic field of the TM incident wave remains unchanged with varying incident angles, which can effectively drive a current loop circulating the cavity, and thus, the angle dependence of its resonant wavelength is significantly weak.

Compared to GPAs using the patterned dielectric structures of Figure 4, a wider absorption bandwidth is obtained at the cost of high ohmic loss in noble metals.

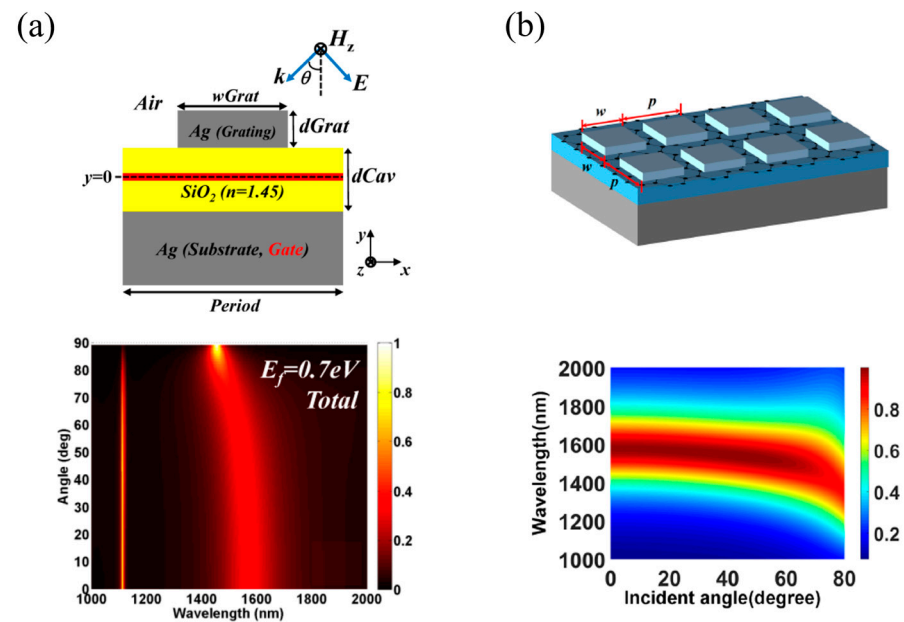


Figure 5. Angle-insensitive absorption based on GPAs using unpatterned graphene and periodic metal nanocavity. (a) Top: schematic of a GPA consisting of monolayer ENZ graphene embedded in metal nanocavity with silver ribbons. Bottom: absorption spectra as a function of incident angle for TM polarization at $E_f = 0.7$ eV [23]. (b) Top: schematic of a GPA consisting of monolayer dielectric graphene embedded in metal nanocavity with square silver plates. Bottom: absorption spectra as a function of incident angle for TM polarization [31]. Reproduced with permission from [23,31], © 2023 Optical Society of America; © 2023 Springer Nature.

2.2.2. Ultra-Broadband Absorption

In general, a fundamental trade-off exists between the bandwidth and amplitude of attainable absorption. To achieve both broadband and high absorption, it is crucial to employ multiple resonances. In this subsection, we focus on ultra-broadband absorber structures, wherein various resonant modes are superimposed upon one another. The graphene-based ultra-broadband absorbers are highly desirable for some applications such as photovoltaics, photodetectors, and thermal emitters.

Firstly, monolayer graphene-based ultra-broadband absorbers are reviewed. One effective method is to use unpatterned monolayer graphene sandwiched between a periodic structure consisting of dielectric or metal (for example, 1D gratings with isosceles trapezoid cross section [63], bricks arrays [64], elliptical cylinder arrays [65], and multi-circular gold patches of different radii [66], snowflake Koch Fractal (SKF) [67]) and a dielectric spacer on top of a metal reflector. In particular, in ref. [63] (Figure 6a), due to the coupling between Mie resonances with graphene plasmon resonance, a flat-top absorption spectrum (in detail, above 99% absorption covers the frequency ranges of 0.66–1.21 THz, and the fractional bandwidth reaches about 60%) is demonstrated. In 2019, Basiri et al. [67] introduced an ultra-wideband THz metamaterial absorber based on SKF dielectric loaded on a graphene sheet. For both TE and TM polarizations, ~160% fractional bandwidth is achieved while attaining over 90% absorption. Another alternative method to accomplish broadband absorption could be the utilization of multi-resonances of patterned monolayer graphene. For example, by applying the graphene concentric double rings [68], graphene ribbons with gradient width [69], sinusoidal-patterned graphene [70] (Figure 6b), complementary cross-oval-shaped graphene [71], and slotted-square graphene meta-rings [72], several or continuous graphene plasmon resonances can be excited over a broadband wavelength

range. In 2023, Massoud et al. [72] proposed the polarization-insensitive, broadband THz absorber comprising a simple meta-square ring of graphene, which possesses different slots in its structure to induce multiple plasmonic resonances. Above 95% absorption covers the frequency ranges of 2.2–4.6 THz, and thus, the fractional bandwidth reaches ~70%.

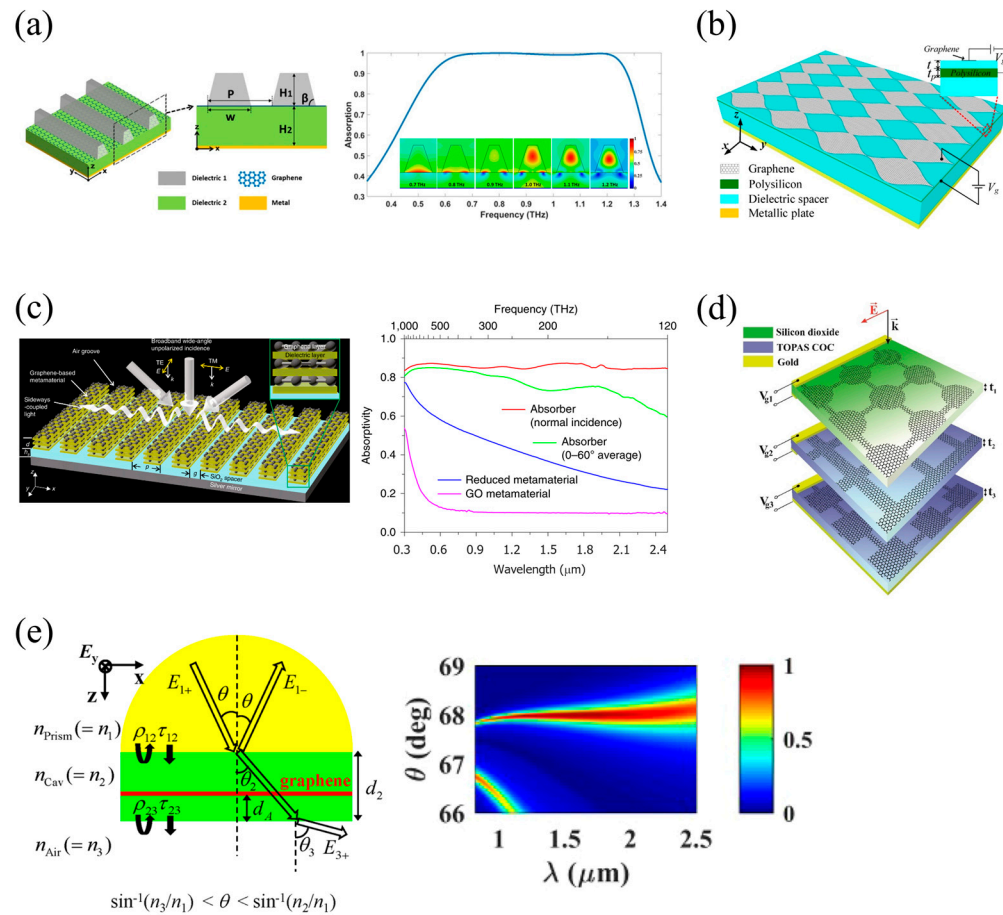


Figure 6. GPAs with ultra-broadband absorption. (a) Left: schematic of a GPA consisting of unpatterned monolayer graphene and 1D gratings with isosceles trapezoid cross section. Right: absorption spectra at $E_f = 0.3$ eV. Inset show magnetic field amplitude for six representative frequencies in the 99% absorption band [63]. (b) Schematic of a GPA consisting of sinusoidal-patterned graphene [70]. (c) Left: schematic of a GPA consisting of alternating graphene and dielectric layers with 1D air grooves, forming a grating. Right: absorption spectra at normal incidence of proposed graphene metamaterial absorber (red), an absorber with angle-averaged absorption from 0 to 60° (green) [73]. (d) Schematic of a GPA consisting of three-layer structure with square-, cross-, and circular-shaped graphene metasurfaces [75]. (e) Left: schematic of a GPA designed for ultra-wide bandwidth absorption based on wavelength-insensitive phase matching. Right: absorption spectra as a function of incident angle [44]. Reproduced with permission from [44,63,70,73,75], © 2023 Optical Society of America; © 2023 Optical Society of America; © 2023 Springer Nature; © 2023 Optical Society of America; © 2023 Springer Nature.

Secondly, mutli-layer graphene can be used to obtain ultra-broadband absorption. In 2019, Jia et al. [73] experimentally demonstrated a 90 nm thick graphene metamaterial with grating, which consists of alternating graphene and dielectric layers (Figure 6c). The grating couples the light sideways into waveguide modes that propagate along the surface, leading to large absorption in the metamaterial. The absorber has broad-bandwidth absorption of well over 80% of non-polarized light over almost the entire solar spectrum (300–2500 nm). Yao et al. [74] showed that the absorption efficiency of the proposed absorber can be as high as more than 90% over 2.10 THz (from 6.98 to 9.10 THz). From top to bottom, the

structure consists of a periodical graphene pattern and a double-layer graphene sheet (the two layers of graphene sheets are unpatterned graphene planes) sandwiched with a silicon dioxide layer and the gold ground plane, tightly stacked to form the unit cell. In 2018, Abdolali et al. [75] demonstrated that the proposed absorber exhibits an absorption of >90% in an ultra-broad range of 0.55–3.12 THz. The proposed absorber is a compact, three-layer structure, comprising square-, cross-, and circular-shaped graphene metasurfaces embedded between three separator dielectrics, and all of them are backed by a metal reflector (Figure 6d). Chen et al. [76] introduced a broadband THz absorber with an array of graphene-dielectric multilayered pyramids on a metal reflector. High absorption with an ultra-broad bandwidth from 8 THz to over 100 THz is achieved due to squeezing graphene plasmons at different levels of the gradually tapered pyramid stack, similarly to sawtooth anisotropic hyperbolic metamaterial absorbers in ref. [77].

Thirdly, the prism-coupling absorber scheme can be also utilized for ultra-broadband absorption. Kim et al. [44] proposed GPAs of ultra-wide bandwidths based on prism coupling with wavelength-insensitive phase matching, which consists of three dielectric layers (prism–cavity–air) with monolayer graphene embedded in the cavity layer (Figure 6e). Due to inherent material dispersion of the dielectric layers in near-IR regime, with the proper choice of the incidence angle and the cavity thickness, the proposed perfect absorbers can satisfy the phase matching condition over a wide wavelength range, inducing enormous enhancement of the absorption bandwidth. According to theoretical investigation, 99% absorption bandwidth of ~300 nm with perfect absorption at $\lambda = 1.51 \mu\text{m}$ can be achieved, which is ~7 times wider than the conceptual design based on the non-dispersive materials.

3. Graphene Perfect Absorbers without External Mirror

As mentioned in the previous section, back-reflection mirrors are often either lossy (e.g., metallic mirrors) or require additional fabrication efforts (e.g., DBR). Therefore, under single-sided illumination, the possibility of achieving perfect absorption without the aid of backing mirrors is highly attractive and could open up many engineering possibilities [45]. Over the past decade, three types of GPAs schemes without external mirror have been proposed: ‘Degenerate critical coupling absorber’, ‘All-pass filter-based absorber’, and ‘One-port mimicking absorber’.

3.1. ‘Degenerate Critical Coupling Absorber’ Scheme

If a mirror-symmetric two-port resonator supports a single resonance, then at most 50% of the incident power can be absorbed when the system is illuminated from a single side. In 2014, however, Fan et al. [80] theoretically demonstrated that the perfect absorption can be achieved through degenerate critical coupling with two resonant modes of opposite symmetry, which are each responsible for 50% absorption (Figure 7a). The proposed resonator consists of a graphene layer placed on top of a photonic crystal slab. When we assume that the loss of graphene does not change the underlying symmetry of the resonator, according to CMT, the total absorption in the system is given by

$$A(\omega) = \sum_{j=1}^2 \frac{2\gamma_{leak,j}\gamma_{loss,j}}{(\omega - \omega_j)^2 + (\gamma_{leak,j} + \gamma_{loss,j})^2} \quad (2)$$

where the loss of each mode remains independent and total absorption is the sum of the contribution of each mode. Each of the two terms of in Equation (2) will attain a maximum of 50% when the leakage rate of the mode exactly matches the loss rate of graphene at each resonance ($\omega = \omega_j$, $\gamma_{leak,j} = \gamma_{loss,j}$). If the two modes are degenerate ($\omega_1 = \omega_2$), the entire system reaches the so-called degenerate critical coupling, and 100% absorption will be achieved. As shown in Figure 7a, at the point of the mode crossing, the conditions for degenerate critical coupling can be fulfilled, giving rise to the perfect absorption of the structure, thus breaking the limit of 50% absorption. But in reality, it is very difficult to

simultaneously satisfy the frequency degeneracy and the critical coupling conditions of dual modes.

Recently, ultrathin all-dielectric Huygens' metasurfaces have also been proposed for perfect absorption based on degenerate critical coupling [81–87], although graphene is not used as an absorbing medium. By overlapping two orthogonal Mie resonance (such as one electric dipole (ED) and one magnetic dipole (MD) resonance), perfect absorption can be achieved. In 2018, Qiu et al. [83] verified the principle of perfect absorption for all-dielectric metasurfaces based on Ge disks (Figure 7b): the destructive interference between simultaneously excited electric and magnetic dipoles inside each element in the backward direction (known as Kerker condition) in combination with the destructive interference between the scattered field and the incident field in the forward direction. In comparison to photonic crystal slab or grating configurations [80], metasurfaces are more useful for individual tuning of the leakage rates of resonant modes by adjusting the geometrical parameters of each element. In particular, to address the issue of only a moderate quality factor ($Q \sim 10$) resulting from the high radiative loss of Mie resonance, Qiu et al. also adopted the quasi-bound states in the continuum (quasi-BIC) resonance, thereby achieving high- Q (~ 640) near-unity absorption in the near-infrared regime [84]. These all-dielectric Huygens' metasurfaces would offer a new route for mirror-less GPA.

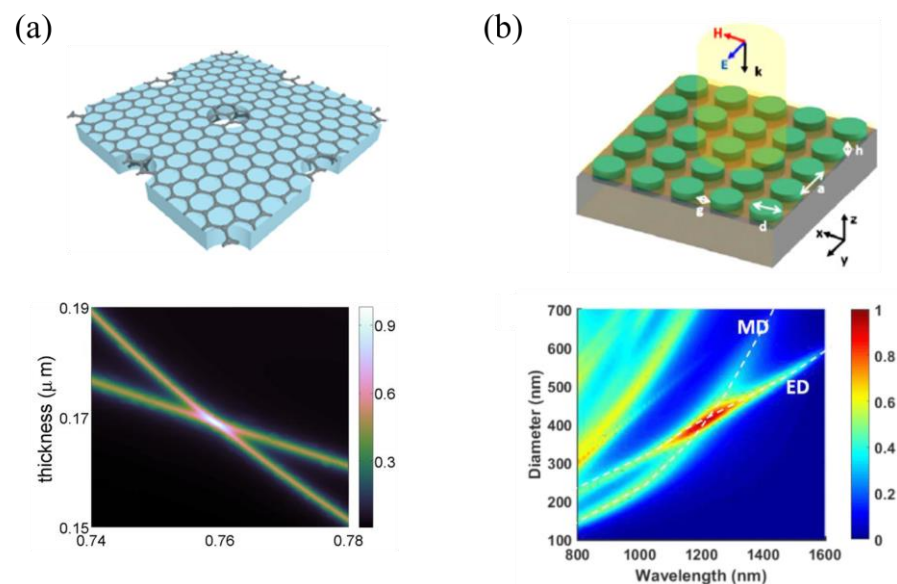


Figure 7. Perfect absorbers based on degenerate critical coupling. (a) Top: schematic of a GPA consisting of monolayer graphene placed on top of a photonic crystal slab. Bottom: absorption spectra as a function of slab thickness [80]. (b) Top: schematic of a PA consisting of Ge disks. Bottom: absorption spectra as a function of disk diameter [83]. Reproduced with permission from [80,83], © 2023 AIP Publishing LLC; © 2023 WILEY-VCH.

3.2. 'All-Pass Filter-Based Absorber' Scheme

Most of the THz PAs that have been proposed thus far are of the reflection type. As a result, the relevant modulators are also of the reflection type, meaning that only the reflected wave can be modulated. In 2019, Kim et al. [88] proposed a GPA scheme employing an all-pass filter such that it functions as a highly efficient transmissive modulator in the THz range (Figure 8). All-pass filter generates a very rapid change from 0 to 360 degree in the vicinity of the resonance while maintaining a unity transmission efficiency, and in general, it is necessary to use at least two resonances (or resonators) [89–92]. In ref. [88], the proposed absorber is composed of two coupled grating resonators with mirror inversion-symmetry as a pure all-pass filter, and the graphene layers are added to introduce loss (Figure 8a). They also theoretically analyzed the proposed scheme using the temporal coupled mode

theory. The two resonators are coupled both indirectly, through the propagation channel with a phase retardation of θ , and directly, through evanescent coupling with a coupling coefficient of μ (Figure 8b). The perfect absorption is obtained when $\theta = \pi/2$, $\mu = 2/\tau$, and $\tau_{L1} = \tau_{L2} = \tau/2$, which is completely different from degenerate critical coupling condition [80] because the suggested absorber scheme considers the coupling of two identical resonators. At the optimal structure, a considerably high modulation depth (~ 70 dB) is achieved via graphene chemical potential variation of ~ 0.15 eV because the proposed transmissive modulator scheme is based on the low transmission state of the near perfect absorption ($\sim 99.8\%$) (Figure 8c,d). In ref. [45], there is another type of PA scheme with a similar inversion symmetry, in which a two-resonance, four-port model is required. Two opposite-direction propagation modes with nonzero in-plane momentum were considered. However, the design and fabrication of the structure will be rather complicated because the scheme works only for an oblique incident angle.

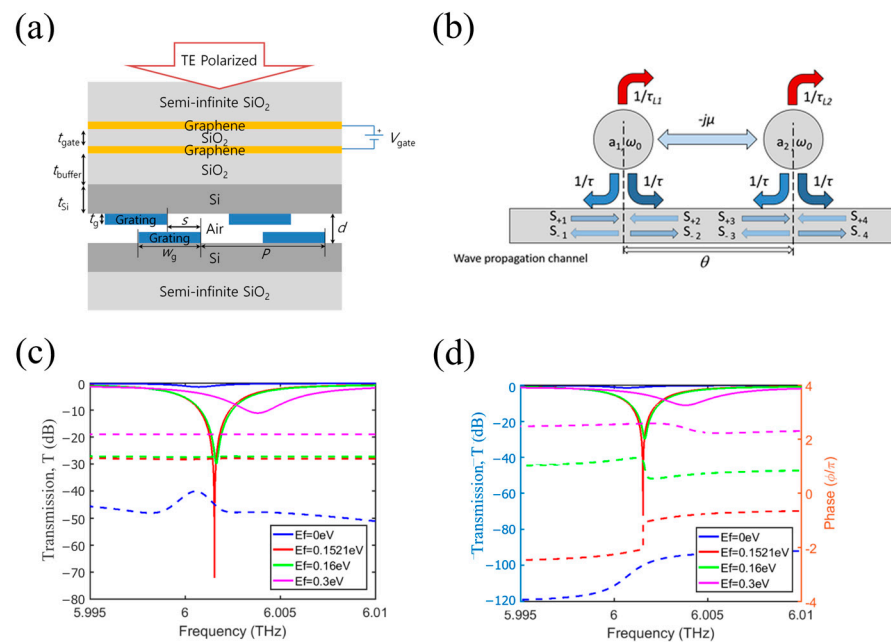


Figure 8. GPA based on all-pass filter, which consists of two coupled grating resonators with mirror inversion-symmetry and graphene absorbing layers. (a) Schematic of the GPA. (b) Theoretical model of the coupled resonators for coupled mode theory analysis. (c) Transmission (solid line) and reflection (dashed line) spectra for different E_f . (d) Transmission (solid line) and phase shift (dashed line) for different E_f . Reproduced with permission from [88], © 2023 Springer Nature.

3.3. ‘One-Port Mimicking Absorber’ Scheme

As aforementioned, the mirror-less GPA is extremely desirable for circumventing numerous limitations associated with the use of the external mirror such as DBR or metal reflector. As an alternative, one-port mimicking absorber scheme is conceptually to mimic a single-mode/mirror system by introducing the internal (or virtual) mirror in a two-port system, and thus the relevant absorption efficiency can be approximately described as Equation (1). In 2017, Kim et al. [46] proposed a novel device structure for the perfect absorption of single-sided illumination, which consists of a high-contrast grating (HCG) with a broadband reflection spectrum, a slab separated by a gap region, and monolayer graphene placed just below the slab (Figure 9). In the CMT analysis, the authors treated the HCG as a lossless resonator with two nondegenerate resonance modes with high leakage rates γ_1 and γ_2 and resonance frequencies ω_1 and ω_2 , respectively, while the slab with a graphene layer is treated as a lossy single-mode resonator with a low leakage rate γ_3 , a loss rate γ_{loss} , and a resonance frequency ω_3 (Figure 9b). The proposed scheme can be dubbed ‘triple-mode absorber’. The perfect absorption is obtained through proper direct

and indirect coupling between the HCG and slab, by which the HCG (as a 100% internal mirror) and slab (as a single-mode resonator) act as single-mode/mirror system, that is, one-port mimicking. Regardless of the existence of graphene layer, transmission becomes zero. The proposed absorber provides excellent tolerance to structural parameters and graphene quality due to the strong field enhancement in the slab region (Figure 9d). Also, absorption spectrum tuning over a wider wavelength range of ~300 nm is possible, keeping significantly high maximum absorption (>95%). These results mean that the proposed scheme significantly relieve the complexity of absorber design compared to the degenerate critical coupling absorber (or dual-mode absorber) [80] because the frequency degeneracy condition is no longer required.

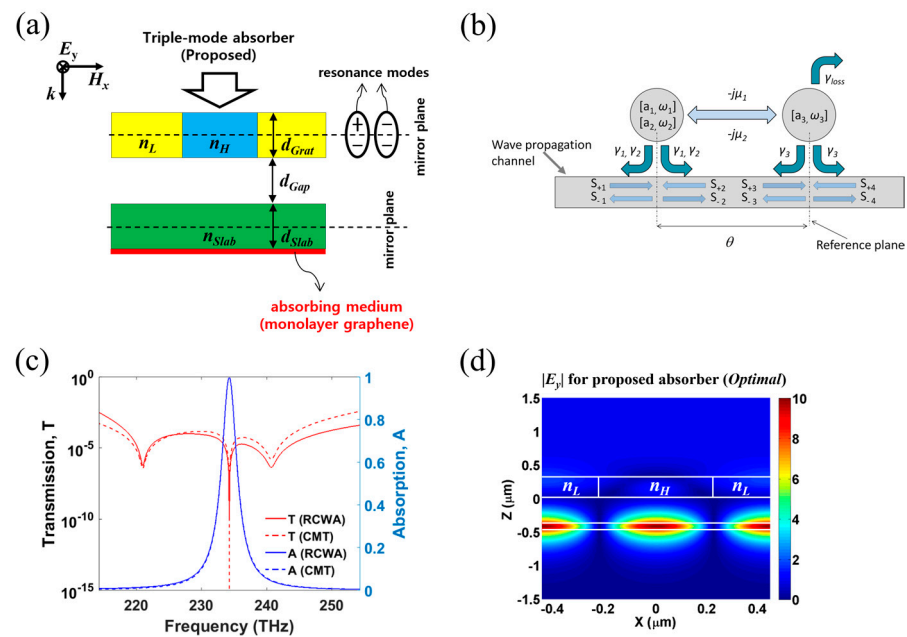


Figure 9. GPA based on one-port mimicking, which consists of a high-contrast grating, a slab separated by a gap region, and monolayer graphene placed just below the slab. (a) Schematic of the GPA. (b) Theoretical model for coupled mode theory analysis. (c) Comparison of RCWA and CMT results. (d) Electric field distribution at optimal condition. Reproduced with permission from [46], © 2023 Springer Nature.

Recently, Kim et al. [47] proposed one-port mimicking scheme in an asymmetric single resonator supporting two degenerate resonant modes (Figure 10). Although the two coupled resonator-based PA scheme mimicking the one-port system has many advantages [46], in general, a single resonator-based structure is preferred in terms of fabrication simplicity if no specific structural symmetry is required [47–49]. In the designed GPA with undoped monolayer graphene placed on a slab-waveguide grating (SWG), only one of the guided-mode resonance modes (GMR₂₁) is responsible for absorption, while the other (GMR₁₃) plays as an internal 100% mirror in conjunction with the Fabry–Perot-like background scattering. The operation concept was confirmed through CMT analysis (Figure 10b). Almost perfect absorption ($A > 99.95\%$) was achieved at the resonant wavelength of the high-Q GMR₂₁ mode. Unlike the degenerate critical coupling absorber [80], the proposed SWG structure is vertically asymmetric, and thus, two degenerate resonant modes (that is, GMR₁₃ and GMR₂₁) are indirectly (not directly) coupled due to partial reflection in the internal wave propagation channel (Figure 10c). The designed device also showed enhanced fabrication error tolerance, which was approximately an order of magnitude larger compared to the scheme based on degenerate critical coupling [80]. Since the proposed GPA structure does not require any structural symmetry, its design is straightforward, and its fabrication will be easier.

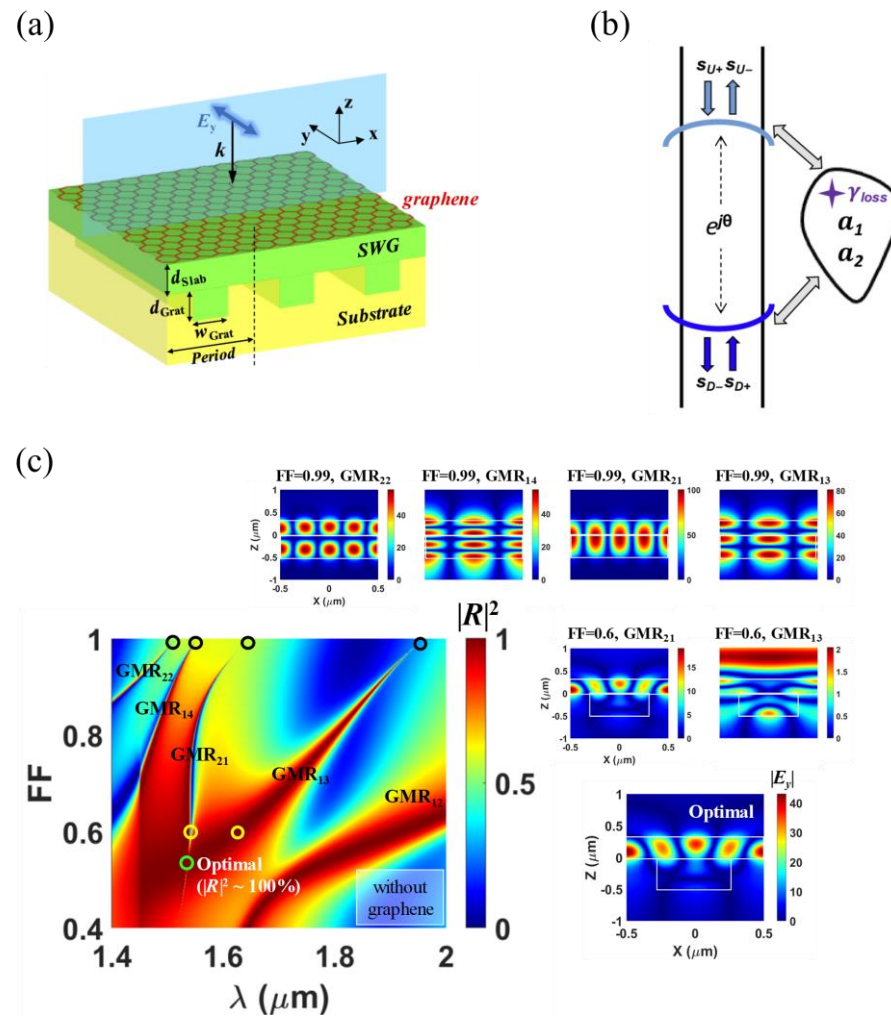


Figure 10. GPA based on one-port mimicking, which consists of an asymmetric single resonator supporting two degenerate resonant modes. (a) Schematic of the GPA. (b) Theoretical model for coupled mode theory analysis. (c) Reflection map as a function of FF when only the graphene is removed for optimized graphene perfect absorber. The inset shows the normalized electric field distribution at seven different points marked by open circles. Reproduced with permission from [47], © 2023 Optical Society of America.

In the GPA design, the critical coupling condition is a common and essential requirement. Mostly, the leakage rate of any resonant mode can hardly be adjusted after device fabrication because it is determined by structural parameters. On the other hand, due to the difficulty of the precise control of the quality of synthesized graphene and unwanted doping in graphene transferred to the substrate, the loss rate of graphene is rather unpredictable, so that the perfect absorption is quite difficult to achieve in practice. To solve this problem, in 2021, Kim et al. [49] proposed the GPA with a loss-adaptive Q -factor control function enabled by quasi-BIC, in which its leakage rate is adapted to the loss rate by a proper choice of the incident angle (Figure 11). The proposed absorber consisting of monolayer graphene placed on an SWG that supports both quasi-BIC and GMR. Similarly to the one-port mimicking scheme in asymmetric resonators of [47,48], the quasi-BIC (in detail, BIC2nd) is responsible for absorption, while the GMR (in detail, GMR1st) works as an internal mirror. Another outstanding feature of the proposed PA is remarkably uncomplicated manufacturing process since absorbing medium (including graphene) is placed on the ridge side of the SWG. Moreover, the proposed device scheme can have an arbitrarily

small leakage rate via adaptive control of the incident angle, and thus, it can be used to implement a PA for any kind of ultrathin absorbing media.

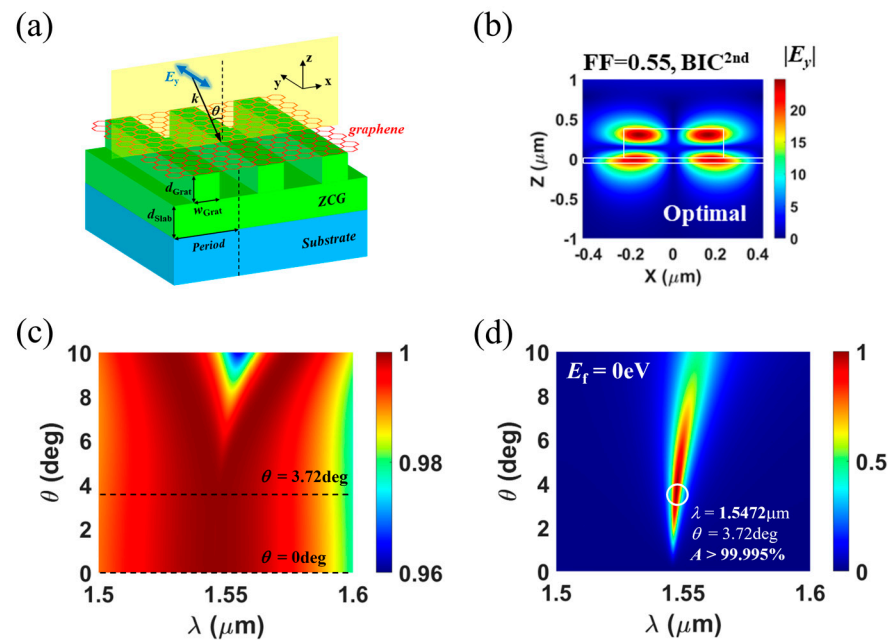


Figure 11. GPA based on one-port mimicking, which consists of a monolayer graphene placed on a SWG that supports both quasi-BIC and GMR. (a) Schematic of the GPA. (b) Electric field distribution at optimal condition. (c) Reflection spectra as a function of incident angle without graphene. (d) Absorption spectra as a function of incident angle with graphene. Perfect absorption point is marked by the white open circle. Reproduced with permission from [49], © 2023 Springer Nature.

4. Applications

Until now, practical applications of GPAs have yet to reach a state of maturity. In this section, we briefly introduce a few optoelectronic applications of GPA structures using external mirrors. Figure 12a indicates the schematic depiction of the possible applications, such as high-efficiency modulators [14,15,36,93–95], photodetectors [12,13,16], tunable polarizers [96–98], switches [99–103], and sensors [104–106].

To create the optical modulator based on an electrically tunable GPA, in 2014, Capasso et al. [14] proposed a widely tunable metasurface composed of optical antennas on graphene, which is incorporated into an ultrathin ($<\lambda_0/10$) optical cavity (Figure 12b). By switching the GPA in and out of the critical coupling condition via the gate voltage applied on graphene, a maximum modulation depth over 95% and modulation speed up to 20 GHz over a mid-IR range can be achieved. The operation wavelength can be scaled from the near-IR to THz ranges due to the great flexibility in tailoring the response of metasurfaces combined with the broadband optical response of graphene.

In 2012, Mueller et al. [16] reported that by monolithically integrating graphene with a Fabry–Perot microcavity with a high finesse, compared to the $\sim 2.3\%$ absorption of free-standing graphene, the optical absorption is 26-fold enhanced at ~ 850 nm wavelength, as shown in Figure 12c. The absorbing graphene layer is sandwiched between two DBR mirrors. A buffer layer ensures that the maximum of the field amplitude occurs right at the position where the graphene sheet is placed. In particular, for bilayer graphene, a maximum responsivity of 21 mA/W is achieved.

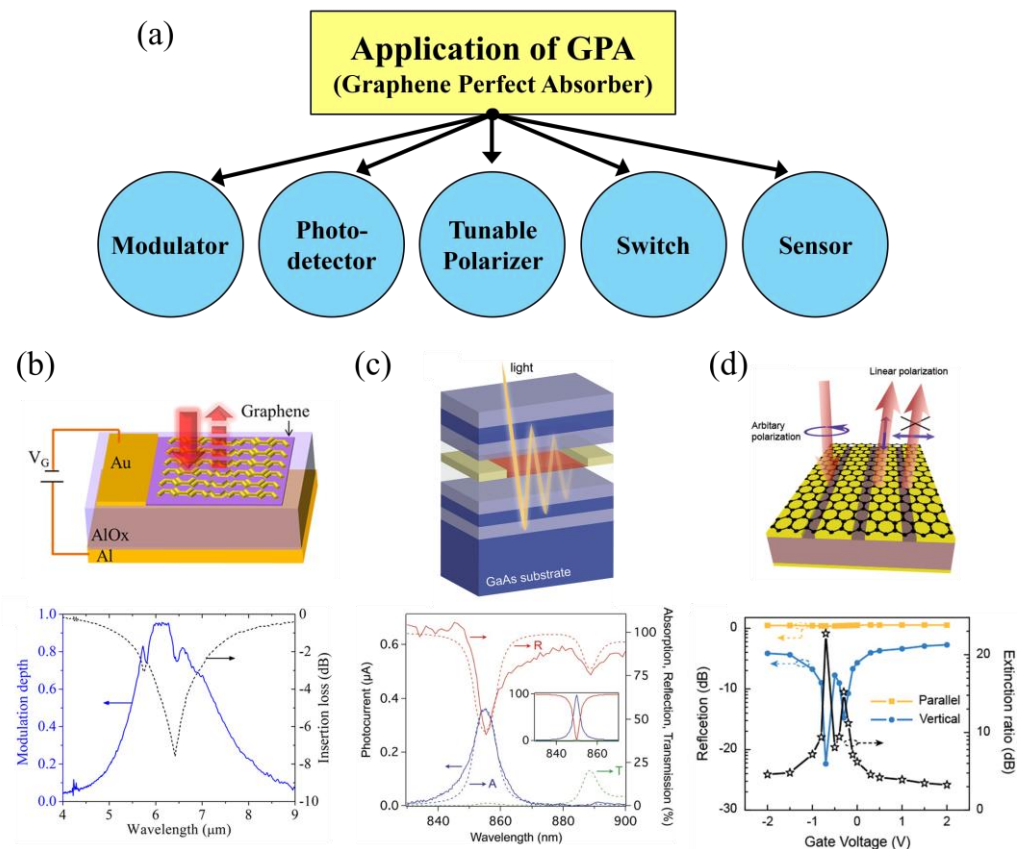


Figure 12. Application of GPA. (a) Schematic of the possible applications of GPA using external mirrors. (b) Top: schematic of the ultrathin optical modulator based on a tunable metasurface absorber backed by Al substrate. Bottom: modulation depth achieved experimentally at different wavelength and corresponding insertion loss [14]. (c) Top: schematic of a graphene microcavity photodetector using two DBRs. The incident light is trapped in the cavity and passes multiple times through the graphene. The graphene sheet is shown in red, and the metal contacts are in yellow. Bottom: spectral response of the monolayer graphene device. The dashed lines show calculation results: reflection R (red), transmission T (green), and absorption A (blue). The solid lines are measurement results: reflection (red), photocurrent (blue). Inset: Theoretical result for normal incidence light [16]. (d) Top: schematic of the electrically tunable polarizer based on the graphene–grating hybrid metasurface. Bottom: measured reflection under parallel (yellow) and vertical (blue) polarizations of the incident THz field as a function of gate voltage at 0.43 THz and the corresponding extinction ratio (black) [96]. Reproduced with permission from [14,16,96], © 2023 American Chemical Society; © 2023 American Chemical Society; © 2023 WILEY-VCH.

In 2020, Zhang et al. [96] experimentally demonstrated an electrically tunable perfect absorber at 0.43 THz by integrating a metallic grating into a graphene-based Salisbury screen structure (Figure 12d). In particular, polarization-dependent reflection of the hybrid absorber was investigated. The measured results reveal that the reflection remains nearly 1 under different gate voltages when the polarization of the incident THz field is parallel to the gate grating, while the reflection can be electrically tuned from 0.5 to nearly 0 for the crossing polarization. Therefore, the proposed graphene–grating hybrid metasurface is highly anisotropic and able to function as an electrically tunable THz polarizer with an extinction ratio up to 23 dB.

In particular, the GPAs based on dielectric resonant structures have the potential for sensing or switching applications because they can minimize the undesired ohmic loss in metals, and even ultra-narrow ($Q > 10,000$) graphene perfect absorption can be achieved [28,33,102,103]. For example, in 2020, Tang et al. [103] numerically demonstrated

a GPA structure with a record-breaking Q -factor (up to 10^5), which is one or two orders of magnitude larger than that of the conventional GPAs. An unpatterned monolayer graphene is placed between the periodic dielectric nanowires and DBR layers. The ultra-low leakage rate of the quasi-BIC resonator and the ultra-low loss rate in the graphene layer are the main contributions for the ultra-high Q perfect absorption. The sensitivity (S) of a spectral wavelength shift for the refractive index change in the resonator is up to 915 nm/RIU, and the figure of merit ($FOM = S/FWHM$) is $\sim 5 \times 10^4$, providing the possibility for applications in all-optical switches when a *Kerr* nonlinear medium is introduced.

5. Conclusions and Perspectives

In this topical review, we briefly summarized the recent advancements of the GPAs with external mirror and without external mirror, focusing mainly on their operation principle and design requirement. Graphene is a very attractive material for optoelectronic devices due to its remarkable carrier mobility and broad absorption band. However, because its potential use is limited by low absorption of graphene, GPA is the first step to approach practical application. Until now, numerous studies for enhancing graphene absorption have been reported, but there is still considerable room to develop the perfect graphene absorbers based on the different schemes investigated in this review paper.

Table 1 presents a comprehensive summary of the key parameters governing the absorption performance of representative GPAs, including the state-of-the-art technology GPAs. Actually, experimental achievements have been limited to the GPAs with an external mirror. For example, as shown in Figure 4b, for monolayer graphene coupled with subwavelength PMMA gratings on top of a back gold mirror, peak absorptions over 99% at a wavelength of ~ 1500 nm with FWHM about 20 nm were measured, which are in excellent quantitative agreement with the simulation results [29]. In 2021, Grilli et al. [107] demonstrated experimentally for the first time a great enhancement in absorption in large-area (1 in diameter) monolayer CVD graphene by exploiting the electric field inside an asymmetric Fabry–Perot resonator fabricated by RF sputtering. The measured absorption of 84% that peaked at 3150 nm with a bandwidth of 44 nm is in very good agreement with COMSOL Multiphysics calculations. In 2023, Chen et al. [108] proposed the photodetector structure using Tamm plasmon by combining a metal film and a DBR, where graphene was transferred onto the DBR, and a metal film was fabricated on the graphene layer. A strong localized field is generated by the structure and detected by graphene, which converted to the photocurrent response. So, the responsivity of the photodetector can be affected by the absorption of the structure. In detail, a maximum absorption of $\sim 60\%$ and responsivity of $\sim 330 \mu\text{A/W}$ are measured at an incident angle of 50 degrees and a wavelength of ~ 850 nm. The difference in reflectance (or absorption) between the experiment and simulation can be observed, which is caused by the error in the thickness of the metal film in the fabrication process.

Table 1. Summary of the key absorption performance parameters of representative GPAs.

Structure	Wavelength or Frequency	Absorption Efficiency (%)	FWHM	Fractional Bandwidth (%)	Sim. or Exp.	Ref.
with external mirror	~ 1500 nm	99.6	~ 5.5 nm	—	Sim.	[24]
	1306 nm	99.4	~ 0.5 nm	—	Sim.	[39]
	1586 nm	95.52	~ 35 nm	—	Sim.	[54]
	~ 1606 nm	~ 95.8	~ 0.018 nm	—	Sim.	[103]
	$\sim 7 \mu\text{m}$	~ 100	$\sim 1.5 \mu\text{m}$	—	Exp.	[14]
	$\sim 13 \mu\text{m}$	77.6	$\sim 1 \mu\text{m}$	—	Exp.	[18]
	1526.5 nm	99	~ 18 nm	—	Exp.	[25]
	1507 nm	96	~ 3 nm	—	Exp.	[26]
	~ 1545 nm	85	~ 3.5 nm	—	Exp.	[27]
	1483.5 nm	~ 99	~ 20 nm	—	Exp.	[29]
	650 nm	86.1	~ 314 nm	—	Exp.	[43]

Table 1. Cont.

Structure	Wavelength or Frequency	Absorption Efficiency (%)	FWHM	Fractional Bandwidth (%)	Sim. or Exp.	Ref.
with external mirror	~3150 nm	84	~44 nm	—	Exp.	[107]
	~850 nm	~60	~15 nm	—	Exp.	[108]
	~8.5 μm	94	~2 μm	—	Exp.	[109]
	1370–1670 nm	>99	—	~20	Sim.	[44]
	0.66–1.21 THz	>99	—	~60	Sim.	[63]
	2.20–4.60 THz	>95	—	~70	Sim.	[72]
	6.98–9.10 THz	>90	—	~26	Sim.	[74]
	2.50–3.80 THz	>90	—	~43	Sim.	[69]
	0.55–3.12 THz	>90	—	~140	Sim.	[75]
	0.88–8.12 THz	>90	—	~160	Sim.	[67]
300–2500 nm	>85	—	~157	Exp.	[73]	
without external mirror	1320 nm	~98	~6 nm	—	Sim.	[80]
	~50 μm	99.8	~40 nm	—	Sim.	[88]
	~1281 nm	~100	~16 nm	—	Sim.	[46]
	~1535 nm	99.95	~1.52 nm	—	Sim.	[47]
	~1547 nm	~100	~4.5 nm	—	Sim.	[49]

Among various absorbers discussed in this review, the mirror-less GPAs are expected to be very promising due to their having two key advantages over the conventional absorbers using an external mirror. Firstly, they simplify the design and fabrication of absorber structure due to the absence of DBR, which requires a sophisticated growth technique. Secondly, they improve net absorption in the graphene layer because the parasitic absorption such as ohmic loss in metal mirror is minimized. In particular, it is noteworthy that the mirror-less absorbers based on one-port mimicking scheme do not require strict structural symmetry, and thus, the limitation on material index choice is greatly relieved. Adopting a novel all-dielectric Huygens' metasurface, which offers easy individual tuning of the relevant resonant modes by adjusting geometrical parameters of each element, would offer a new route for mirror-less GPAs. Another prospective research direction is to introduce mechanical flexibility in GPAs by utilizing flexible substrate. Graphene produced via CVD can be transferred to different polymers, such as polyethylene terephthalate (PET), polyimide (PI), and polydimethylsiloxane (PDMS), which are the most commonly used flexible substrates because these have unique flexibility, high mechanical stability, and high chemical stability [110,111]. For example, in 2019, by using a graphene FSS (frequency-selective surface) combined with an oxide-metal-oxide film fabricated on a PET substrate, Jiang et al. [112] showed that the graphene absorber structure with good flexibility can provide a wideband absorption in microwave regime.

Author Contributions: Conceptualization, S.L. and S.K.; writing—original draft preparation, S.L.; writing—review and editing, S.K.; visualization, S.L.; supervision, S.K.; funding acquisition, S.K. All authors have read and agreed to the published version of the manuscript.

Funding: This research was funded by the National Research Foundation of Korea (2021R1A4A1033155).

Conflicts of Interest: The authors declare no conflict of interest.

References

- Watts, C.M.; Liu, X.; Padilla, W.J. Metamaterial Electromagnetic Wave Absorbers. *Adv. Mater.* **2012**, *24*, OP98–OP120. [CrossRef]
- Cui, Y.; He, Y.; Jin, Y.; Ding, F.; Yang, L.; Ye, Y.; Zhong, S.; Lin, Y.; He, S. Plasmonic and metamaterial structures as electromagnetic absorbers. *Laser Photonics Rev.* **2014**, *8*, 495–520. [CrossRef]
- Ogawa, S.; Kimata, M. Metal-Insulator-Metal-Based Plasmonic Metamaterial Absorbers at Visible and Infrared Wavelengths: A Review. *Materials* **2018**, *11*, 458. [CrossRef]
- Yu, P.; Besteiro, L.V.; Huang, Y.; Wu, J.; Fu, L.; Tan, H.H.; Jagadish, C.; Wiederrecht, G.P.; Govorov, A.O.; Wang, Z. Broadband Metamaterial Absorbers. *Adv. Opt. Mater.* **2019**, *7*, 1800995. [CrossRef]

5. Yao, Y.; Liao, Z.; Liu, Z.; Liu, X.; Zhou, J.; Liu, G.; Yi, Z.; Wang, J. Recent progresses on metamaterials for optical absorption and sensing: A review. *J. Phys. D Appl. Phys.* **2021**, *54*, 113002. [[CrossRef](#)]
6. Li, Q.; Lu, J.; Gupta, P.; Qiu, M. Engineering Optical Absorption in Graphene and Other 2D Materials: Advances and Applications. *Adv. Opt. Mater.* **2019**, *7*, 1900595. [[CrossRef](#)]
7. Guo, C.; Zhang, J.; Xu, W.; Liu, K.; Yuan, X.; Qin, S.; Zhu, Z. Graphene-Based Perfect Absorption Structures in the Visible to Terahertz Band and Their Optoelectronics Applications. *Nanomaterials* **2018**, *8*, 1033. [[CrossRef](#)] [[PubMed](#)]
8. Hajian, H.; Ghobadi, A.; Butun, B.; Ozbay, E. Active metamaterial nearly perfect light absorbers: A review. *J. Opt. Soc. Am. B* **2019**, *36*, F131–F143. [[CrossRef](#)]
9. Luo, X.; Zhou, Y.; Cai, Y.; Cheng, Z.; Liu, Z.; Wan, W. A review of perfect absorbers based on the two dimensional materials in the visible and near-infrared regimes. *J. Phys. D Appl. Phys.* **2022**, *55*, 093002. [[CrossRef](#)]
10. Nematpour, A.; Grilli, M.L.; Lancellotti, L.; Lisi, N. Towards Perfect Absorption of Single Layer CVD Graphene in an Optical Resonant Cavity. *Materials* **2022**, *15*, 352. [[CrossRef](#)]
11. Nair, R.R.; Blake, P.; Grigorenko, A.N.; Novoselov, K.S.; Booth, T.J.; Stauber, T.; Peres, N.M.; Geim, A.K. Fine structure constant defines visual transparency of graphene. *Science* **2008**, *320*, 1308. [[CrossRef](#)]
12. Mueller, T.; Xia, F.N.; Avouris, P. Graphene photodetectors for high-speed optical communications. *Nat. Photonics* **2010**, *4*, 297–301. [[CrossRef](#)]
13. Liu, C.H.; Chang, Y.C.; Norris, T.B.; Zhong, Z. Graphene photodetectors with ultra-broadband and high responsivity at room temperature. *Nat. Nanotechnol.* **2014**, *9*, 273–278. [[CrossRef](#)]
14. Yao, Y.; Shankar, R.; Kats, M.A.; Song, Y.; Kong, J.; Loncar, M.; Capasso, F. Electrically tunable metasurface perfect absorbers for ultrathin mid-infrared optical modulators. *Nano Lett.* **2014**, *14*, 6526–6532. [[CrossRef](#)] [[PubMed](#)]
15. Kim, S.; Jang, M.S.; Brar, V.W.; Mauser, K.W.; Kim, L.; Atwater, H.A. Electronically Tunable Perfect Absorption in Graphene. *Nano Lett.* **2018**, *18*, 971–979. [[CrossRef](#)]
16. Furchi, M.; Urich, A.; Pospischil, A.; Lilley, G.; Unterrainer, K.; Detz, H.; Klang, P.; Andrews, A.M.; Schrenk, W.; Strasser, G.; et al. Microcavity-integrated graphene photodetector. *Nano Lett.* **2012**, *12*, 2773–2777. [[CrossRef](#)] [[PubMed](#)]
17. Vasić, B.; Gajić, R. Tunable Fabry–Perot resonators with embedded graphene from terahertz to near-infrared frequencies. *Opt. Lett.* **2014**, *39*, 6253–6256. [[CrossRef](#)]
18. Zhu, L.; Liu, F.; Lin, H.; Hu, J.; Yu, Z.; Wang, X.; Fan, S. Angle-selective perfect absorption with two-dimensional materials. *Light Sci. Appl.* **2016**, *5*, e16052. [[CrossRef](#)]
19. Deng, X.-H.; Liu, J.-T.; Yuan, J.; Wang, T.-B.; Liu, N.-H. Tunable THz absorption in graphene-based heterostructures. *Opt. Express* **2014**, *24*, 30177–30183. [[CrossRef](#)]
20. Lu, H.; Gan, X.; Jia, B.; Mao, D.; Zhao, J. Tunable high-efficiency light absorption of monolayer graphene via Tamm plasmon polaritons. *Opt. Lett.* **2016**, *41*, 4743–4746. [[CrossRef](#)]
21. Thongrattanasiri, S.; Koppens, F.H.L.; Garcia de Abajo, F.J. Complete optical absorption in periodically patterned graphene. *Phys. Rev. Lett.* **2012**, *108*, 047401. [[CrossRef](#)] [[PubMed](#)]
22. Liu, X.; Liu, G.; Tang, P.; Fu, G.; Du, G.; Chen, Q.; Liu, Z. Quantitatively optical and electrical-adjusting high-performance switch by graphene plasmonic perfect absorbers. *Carbon* **2018**, *140*, 362–367. [[CrossRef](#)]
23. Lee, S.; Tran, T.Q.; Kim, M.; Heo, H.; Heo, J.; Kim, S. Angle- and position-insensitive electrically tunable absorption in graphene by epsilon-near-zero effect. *Opt. Express* **2015**, *23*, 33350–33358. [[CrossRef](#)] [[PubMed](#)]
24. Piper, J.R.; Fan, S. Total absorption in a graphene monolayer in the optical regime by critical coupling with a photonic crystal guided resonance. *ACS Photonics* **2014**, *1*, 347–353. [[CrossRef](#)]
25. Fan, Y.S.; Guo, C.C.; Zhu, Z.H.; Xu, W.; Wu, F.; Yuan, X.D.; Qin, S.Q. Monolayer-graphene-based perfect absorption structures in the near infrared. *Opt. Express* **2017**, *25*, 13079–13086. [[CrossRef](#)]
26. Wang, W.; Klots, A.; Yang, Y.; Li, W.; Kravchenko, I.I.; Briggs, D.P.; Bolotin, K.I.; Valentine, J. Enhanced absorption in two-dimensional materials via Fano-resonant photonic crystals. *Appl. Phys. Lett.* **2015**, *106*, 181104. [[CrossRef](#)]
27. Liu, Y.; Chadha, A.; Zhao, D.; Piper, J.R.; Jia, Y.; Shuai, Y.; Menon, L.; Yang, H.; Ma, Z.; Fan, S. Approaching total absorption at near infrared in a large area monolayer graphene by critical coupling. *Appl. Phys. Lett.* **2014**, *105*, 181105. [[CrossRef](#)]
28. Long, Y.; Shen, L.; Xu, H.; Deng, H.; Li, Y. Achieving ultranarrow graphene perfect absorbers by exciting guided-mode resonance of one-dimensional photonic crystals. *Sci. Rep.* **2016**, *6*, 32312. [[CrossRef](#)]
29. Guo, C.C.; Zhu, Z.H.; Yuan, X.D.; Ye, W.M.; Liu, K.; Zhang, J.F.; Xu, W.; Qin, S.Q. Experimental Demonstration of Total Absorption over 99% in the Near Infrared for Monolayer-Graphene-Based Subwavelength Structures. *Adv. Opt. Mater.* **2016**, *4*, 1955–1960. [[CrossRef](#)]
30. Zhao, B.; Zhao, J.M.; Zhang, Z.M. Enhancement of near-infrared absorption in graphene with metal gratings. *Appl. Phys. Lett.* **2014**, *105*, 031905. [[CrossRef](#)]
31. Fan, Y.; Guo, C.; Zhu, Z.; Xu, W.; Wu, F.; Yuan, X.; Qin, S. Monolayer-graphene-based broadband and wide-angle perfect absorption structures in the near infrared. *Sci. Rep.* **2018**, *8*, 13709. [[CrossRef](#)] [[PubMed](#)]
32. Mahigir, A.; Veronis, G. Nanostructure for near total light absorption in a monolayer of graphene in the visible. *J. Opt. Soc. Am. B* **2018**, *35*, 3153–3158. [[CrossRef](#)]
33. Lee, S.; Heo, H.; Kim, S. High fabrication-tolerant narrowband perfect graphene absorber based on guided-mode resonance in distributed Bragg reflector. *Sci. Rep.* **2019**, *9*, 4294. [[CrossRef](#)]

34. Alaei, R.; Farhat, M.; Rockstuhl, C.; Lederer, F. A perfect absorber made of a graphene micro-ribbon metamaterial. *Opt. Express* **2012**, *20*, 28017–28024. [[CrossRef](#)]
35. Li, H.; Wang, L.; Zhai, X. Tunable graphene-based mid-infrared plasmonic wide-angle narrowband perfect absorber. *Sci. Rep.* **2016**, *6*, 36651. [[CrossRef](#)]
36. Vasić, B.; Gajić, R. Graphene induced spectral tuning of metamaterial absorbers at mid-infrared frequencies. *Appl. Phys. Lett.* **2013**, *103*, 261111. [[CrossRef](#)]
37. Zhang, Y.; Feng, Y.; Zhu, B.; Zhao, J.; Jiang, T. Graphene based tunable metamaterial absorber and polarization modulation in terahertz frequency. *Opt. Express* **2014**, *22*, 22743–22752. [[CrossRef](#)] [[PubMed](#)]
38. Zhang, Q.; Ma, Q.; Yan, S.; Wu, F.; He, X.; Jiang, J. Tunable terahertz absorption in graphene-based metamaterial. *Opt. Commun.* **2015**, *353*, 70–75. [[CrossRef](#)]
39. Luo, X.; Liu, Z.; Wang, L.; Liu, J.; Lin, Q. Tunable ultra-narrowband and wide-angle graphene-based perfect absorber in the optical communication region. *Appl. Phys. Express* **2018**, *11*, 105102. [[CrossRef](#)]
40. Song, S.; Chen, Q.; Jin, L.; Sun, F. Great light absorption enhancement in a graphene photodetector integrated with a metamaterial perfect absorber. *Nanoscale* **2013**, *5*, 9615–9619. [[CrossRef](#)]
41. Pirruccio, G.; Moreno, L.M.; Lozano, G.; Rivas, J.G. Coherent and broadband enhanced optical absorption in graphene. *ACS Nano* **2013**, *7*, 4810–4817. [[CrossRef](#)] [[PubMed](#)]
42. Lee, S.; Kim, S. Practical Perfect Absorption in Monolayer Graphene by Prism Coupling. *IEEE Photonics J.* **2017**, *9*, 2700810. [[CrossRef](#)]
43. Heo, H.; Lee, S.; Kim, S. Broadband absorption enhancement of monolayer graphene by prism coupling in the visible range. *Carbon* **2019**, *154*, 42–47. [[CrossRef](#)]
44. Lee, S.; Heo, H.; Kim, S. Graphene perfect absorber of ultra-wide bandwidth based on wavelength-insensitive phase matching in prism coupling. *Sci. Rep.* **2019**, *9*, 11967. [[CrossRef](#)]
45. Zhou, H.; Zhen, B.; Hsu, C.W.; Miller, O.D.; Johnson, S.G.; Joannopoulos, J.D.; Soljačić, M. Perfect single-sided radiation and absorption without mirrors. *Optica* **2016**, *3*, 1079. [[CrossRef](#)]
46. Lee, S.; Tran, T.Q.; Heo, H.; Kim, M.; Kim, S. A proposal of a perfect graphene absorber with enhanced design and fabrication tolerance. *Sci. Rep.* **2017**, *7*, 4760. [[CrossRef](#)] [[PubMed](#)]
47. Lee, S.; Song, J.; Kim, S. Graphene perfect absorber design based on an approach of mimicking a one-port system in an asymmetric single resonator. *Opt. Express* **2021**, *29*, 29631–29640. [[CrossRef](#)]
48. Song, J.; Heo, H.; Lee, S.; Kim, S. Mirror-Less Unidirectional Radiation in an Asymmetric Single Resonator. *J. Lightw. Technol.* **2022**, *40*, 5163–5170. [[CrossRef](#)]
49. Lee, S.; Song, J.; Kim, S. Graphene perfect absorber with loss adaptive Q-factor control function enabled by quasi-bound states in the continuum. *Sci. Rep.* **2021**, *11*, 22819. [[CrossRef](#)]
50. Ghivela, G.C.; Sengupta, J. The Promise of Graphene: A Survey of Microwave Devices Based on Graphene. *IEEE Microw. Mag.* **2020**, *21*, 48–65. [[CrossRef](#)]
51. Nematpour, A.; Lisi, N.; Chierchia, R.; Grilli, M.L. Experimental demonstration of mid-IR absorption enhancement in single layer CVD graphene. *Opt. Lett.* **2020**, *45*, 3861–3864. [[CrossRef](#)]
52. Zhang, Y.; Li, T.; Chen, Q.; Zhang, H.; O'Hara, J.F.; Abele, E.; Taylor, A.J.; Chen, H.-T.; Azad, A.K. Independently tunable dual-band perfect absorber based on graphene at mid-infrared frequencies. *Sci. Rep.* **2016**, *5*, 18463. [[CrossRef](#)]
53. Xu, H.; Hu, L.; Lu, Y.; Xu, J.; Chen, Y. Dual-Band Metamaterial Absorbers in the Visible and Near-Infrared Regions. *J. Phys. Chem. C* **2019**, *123*, 10028–10033. [[CrossRef](#)]
54. Zhou, K.; Cheng, Q.; Lu, L.; Li, B.; Song, J.; Luo, Z. Dual-band tunable narrowband near-infrared light trapping control based on a hybrid grating-based Fabry–Perot structure. *Opt. Express* **2020**, *28*, 1647–1656. [[CrossRef](#)] [[PubMed](#)]
55. Yue, J.; Luo, X.; Zhai, X.; Wang, L.L.; Lin, Q. A tunable dual-band graphene-based perfect absorber in the optical communication band. *Opt. Laser Technol.* **2018**, *108*, 404–408. [[CrossRef](#)]
56. Wu, P.; Chen, Z.; Xu, D.; Zhang, C.; Jian, R. A Narrow Dual-Band Monolayer Unpatterned Graphene-Based Perfect Absorber with Critical Coupling in the Near Infrared. *Micromachines* **2020**, *11*, 58. [[CrossRef](#)]
57. Ning, R.; Bao, J.; Jiao, Z.; Xu, Y. Omnidirectional polarization-insensitive tunable absorption in graphene metamaterial of nanodisk structure. *J. Appl. Phys.* **2015**, *118*, 203101. [[CrossRef](#)]
58. Xia, S.X.; Zhai, X.; Huang, Y.; Liu, J.Q.; Wang, L.L.; Wen, S.C. Multi-band perfect plasmonic absorptions using rectangular graphene gratings. *Opt. Lett.* **2017**, *42*, 3052–3055. [[CrossRef](#)]
59. Meng, H.Y.; Wang, L.L.; Liu, G.D.; Xue, X.X.; Lin, Q.; Zhai, X. Tunable graphene-based plasmonic multispectral and narrowband perfect metamaterial absorbers at the mid-infrared region. *Appl. Opt.* **2017**, *56*, 6022–6027. [[CrossRef](#)] [[PubMed](#)]
60. Meng, H.Y.; Xue, X.X.; Lin, Q.; Liu, G.D.; Zhai, X.; Wang, L.L. Tunable and multi-channel perfect absorber based on graphene at mid-infrared region. *Appl. Phys. Express* **2018**, *11*, 052002. [[CrossRef](#)]
61. Wang, J.; Hou, Y. Ultra-multiband absorption enhancement of graphene in a metal-dielectric-graphene sandwich structure covering terahertz to mid-infrared regime. *Opt. Express* **2017**, *25*, 19185–19194. [[CrossRef](#)]
62. Li, H.-J.; Chen, B.; Zhai, X.; Xu, L.; Wang, L.-L. Tunable Ultra-Multispectral Metamaterial Perfect Absorbers Based on Out-of-Plane Metal-Insulator-Graphene Heterostructures. *J. Light. Technol.* **2020**, *38*, 1858–1864. [[CrossRef](#)]

63. Yang, J.; Zhu, Z.; Zhang, J.; Xu, W.; Guo, C.; Liu, K.; Zhu, M.; Chen, H.; Zhang, R.; Yuan, X.; et al. Mie resonance induced broadband near-perfect absorption in nonstructured graphene loaded with periodical dielectric wires. *Opt. Express* **2018**, *26*, 20174–20182. [[CrossRef](#)]
64. Gao, F.; Zhu, Z.H.; Xu, W.; Zhang, J.F.; Guo, C.C.; Liu, K.; Yuan, X.D.; Qin, S.Q. Broadband wave absorption in single-layered and nonstructured graphene based on far-field interaction effect. *Opt. Express* **2017**, *25*, 9579–9586. [[CrossRef](#)] [[PubMed](#)]
65. Yang, J.W.; Zhu, Z.Z.; Zhang, J.F.; Guo, C.C.; Xu, W.; Liu, K.; Yuan, X.D.; Qin, S.Q. Broadband terahertz absorber based on multi-band continuous plasmon resonances in geometrically gradient dielectric-loaded graphene plasmon structure. *Sci. Rep.* **2018**, *8*, 3239. [[CrossRef](#)]
66. Zhang, Y.; Li, Y.; Cao, Y.; Liu, Y.; Zhang, H. Graphene induced tunable and polarization-insensitive broadband metamaterial absorber. *Opt. Commun.* **2017**, *382*, 281–287. [[CrossRef](#)]
67. Nourbakhsh, M.; Zareian-Jahromi, E.; Basiri, R. Ultra-wideband terahertz metamaterial absorber based on Snowflake Koch Fractal dielectric loaded graphene. *Opt. Express* **2019**, *27*, 32958–32969. [[CrossRef](#)]
68. Mou, N.; Sun, S.; Dong, H.; Dong, S.; He, Q.; Zhou, L.; Zhang, L. Hybridization-induced broadband terahertz wave absorption with graphene metasurfaces. *Opt. Express* **2018**, *26*, 11728–11736. [[CrossRef](#)]
69. Zhu, Z.; Guo, C.; Zhang, J.; Liu, K.; Yuan, X.; Qin, S. Broadband single-layered graphene absorber using periodic arrays of graphene ribbons with gradient width. *Appl. Phys. Express* **2015**, *8*, 015102. [[CrossRef](#)]
70. Ye, L.; Chen, Y.; Cai, G.; Liu, N.; Zhu, J.; Song, Z.; Liu, Q. Broadband absorber with periodically sinusoidally-patterned graphene layer in terahertz range. *Opt. Express* **2017**, *25*, 11223–11232. [[CrossRef](#)]
71. Huang, M.L.; Cheng, Y.Z.; Cheng, Z.Z.; Chen, H.R.; Mao, X.S.; Gong, R.Z. Design of a Broadband Tunable Terahertz Metamaterial Absorber Based on Complementary Structural Graphene. *Materials* **2018**, *11*, 540. [[CrossRef](#)]
72. Zakir, S.; Bilal, R.M.H.; Naveed, M.A.; Baqir, M.A.; Khan, M.U.A.; Ali, M.M.; Saeed, M.A.; Mehmood, M.Q.; Massoud, Y. Polarization-Insensitive, Broadband, and Tunable Terahertz Absorber Using Slotted-Square Graphene Meta-Rings. *IEEE Photonics J.* **2023**, *15*, 4600108. [[CrossRef](#)]
73. Lin, H.; Sturmberg, B.C.P.; Lin, K.-T.; Yang, Y.; Zheng, X.; Chong, T.K.; de Sterke, C.M.; Jia, B. A 90-nm-thick graphene metamaterial for strong and extremely broadband absorption of unpolarized light. *Nat. Photonics* **2019**, *13*, 270–276. [[CrossRef](#)]
74. Fu, P.; Liu, F.; Ren, G.J.; Su, F.; Li, D.; Yao, J.Q. A broadband metamaterial absorber based on multi-layer graphene in the terahertz region. *Opt. Commun.* **2018**, *417*, 62–66. [[CrossRef](#)]
75. Rahmzadeh, M.; Rajabalipanah, H.; Abdolali, A. Multilayer graphene-based metasurfaces: Robust design method for extremely broadband, wide-angle, and polarization-insensitive terahertz absorbers. *Appl. Opt.* **2018**, *57*, 959–968. [[CrossRef](#)]
76. He, S.; Chen, T. Broadband THz Absorbers with Graphene-Based Anisotropic Metamaterial Films. *IEEE Trans. Terahertz Sci. Technol.* **2013**, *3*, 757–763. [[CrossRef](#)]
77. Cui, Y.; Fung, K.H.; Xu, J.; Ma, H.; Jin, Y.; He, S.; Fang, N.X. Ultrabroadband light absorption by a sawtooth anisotropic metamaterial slab. *Nano Lett.* **2012**, *12*, 1443–1447. [[CrossRef](#)]
78. Amin, M.; Farhat, M.; Bağcı, H. An ultra-broadband multilayered graphene absorber. *Opt. Express* **2013**, *21*, 29938–29948. [[CrossRef](#)] [[PubMed](#)]
79. Lu, Z.; Zhao, W. Nanoscale electro-optic modulators based on graphene-slot waveguides. *J. Opt. Soc. Am. B* **2012**, *29*, 1490–1496. [[CrossRef](#)]
80. Piper, J.R.; Liu, V.; Fan, S. Total absorption by degenerate critical coupling. *Appl. Phys. Lett.* **2014**, *104*, 251110. [[CrossRef](#)]
81. Ming, X.; Liu, X.; Sun, L.; Padilla, W.J. Degenerate critical coupling in all-dielectric metasurface absorbers. *Opt. Express* **2017**, *25*, 24658–24669. [[CrossRef](#)]
82. Chen, W.; Wang, X.; Duan, J.; Zhou, C.; Liu, T.; Xiao, S. Perfect absorption in free-standing GaAs nanocylinder arrays by degenerate critical coupling. *Opt. Mater.* **2021**, *121*, 111558. [[CrossRef](#)]
83. Tian, J.; Luo, H.; Li, Q.; Pei, X.; Du, K.; Qiu, M. Near-Infrared Super-Absorbing All-Dielectric Metasurface Based on Single-Layer Germanium Nanostructures. *Laser Photonics Rev.* **2018**, *12*, 1800076. [[CrossRef](#)]
84. Tian, J.; Li, Q.; Belov, P.A.; Sinha, R.K.; Qian, W.; Qiu, M. High-Q All-Dielectric Metasurface: Super and Suppressed Optical Absorption. *ACS Photonics* **2020**, *7*, 1436–1443. [[CrossRef](#)]
85. Liu, X.; Fan, K.; Shadrivov, I.V.; Padilla, W.J. Experimental realization of a terahertz all-dielectric metasurface absorber. *Opt. Express* **2017**, *25*, 191–201. [[CrossRef](#)]
86. Xu, R.; Takahara, J. Radiative loss control of an embedded silicon perfect absorber in the visible region. *Opt. Lett.* **2021**, *46*, 805–808. [[CrossRef](#)]
87. Nishida, K.; Sasai, K.; Xu, R.; Yen, T.-H.; Tang, Y.-L.; Takahara, J.; Chu, S.-W. All-optical scattering control in an all-dielectric quasi-perfect absorbing Huygens' metasurface. *Nanophotonics* **2022**, *12*, 139–146. [[CrossRef](#)]
88. Tran, T.Q.; Lee, S.; Kim, S. A graphene-assisted all-pass filter for a tunable terahertz transmissive modulator with near-perfect absorption. *Sci. Rep.* **2019**, *9*, 12558. [[CrossRef](#)]
89. Suh, W.; Fan, S. All-pass transmission or flattop reflection filters using a single photonic crystal slab. *Appl. Phys. Lett.* **2004**, *84*, 4905. [[CrossRef](#)]
90. Suh, W.; Fan, S. Mechanically switchable photonic crystal filter with either all-pass transmission or flat-top reflection characteristics. *Opt. Lett.* **2003**, *28*, 1763–1765. [[CrossRef](#)]

91. Wang, Z.; Fan, S. Compact all-pass filters in photonic crystals as the building block for high-capacity optical delay lines. *Phys. Rev. E* **2003**, *68*, 066616. [[CrossRef](#)] [[PubMed](#)]
92. Suh, W.; Wang, Z.; Fan, S. Temporal coupled-mode theory and the presence of non-orthogonal modes in lossless multimode cavities. *IEEE J. Quantum Electron.* **2004**, *40*, 1511–1518. [[CrossRef](#)]
93. Sherrott, M.C.; Hon, P.W.C.; Fountaine, K.T.; Garcia, J.C.; Ponti, S.M.; Brar, V.W.; Sweatlock, L.A.; Atwater, H.A. Experimental Demonstration of 230° Phase Modulation in Gate-Tunable Graphene-Gold Reconfigurable Mid-Infrared Metasurfaces. *Nano Lett.* **2017**, *17*, 3027–3034. [[CrossRef](#)]
94. Tasolamprou, A.C.; Koulouklidis, A.D.; Daskalaki, C.; Mavidis, C.P.; Kenanakis, G.; Deligeorgis, G.; Viskadourakis, Z.; Kuzhir, P.; Tzortzakakis, S.; Kafesaki, M.; et al. Experimental Demonstration of Ultrafast THz Modulation in a Graphene-Based Thin Film Absorber through Negative Photoinduced Conductivity. *ACS Photonics* **2019**, *6*, 720–727. [[CrossRef](#)]
95. Sensale-Rodriguez, B.; Yan, R.; Rafique, S.; Zhu, M.D.; Li, W.; Liang, X.L.; Gundlach, D.; Protasenko, V.; Kelly, M.M.; Jena, D.; et al. Extraordinary Control of Terahertz Beam Reflectance in Graphene Electro-absorption Modulators. *Nano Lett.* **2012**, *12*, 4518–4522. [[CrossRef](#)] [[PubMed](#)]
96. Chen, X.; Tian, Z.; Lu, Y.; Xu, Y.; Zhang, X.; Ouyang, C.; Gu, J.; Han, J.; Zhang, W. Electrically Tunable Perfect Terahertz Absorber Based on a Graphene Salisbury Screen Hybrid Metasurface. *Adv. Opt. Mater.* **2020**, *8*, 1900660. [[CrossRef](#)]
97. Zhu, Z.H.; Guo, C.C.; Liu, K.; Zhang, J.F.; Ye, W.M.; Yuan, X.D.; Qin, S.Q. Electrically tunable polarizer based on anisotropic absorption of graphene ribbons. *Appl. Phys. A* **2014**, *114*, 1017–1021. [[CrossRef](#)]
98. Zhu, Z.H.; Guo, C.C.; Liu, K.; Zhang, J.F.; Ye, W.M.; Yuan, X.D.; Qin, S.Q. Electrically controlling the polarizing direction of a graphene polarizer. *J. Appl. Phys.* **2014**, *116*, 104304. [[CrossRef](#)]
99. Chen, J.; Chen, S.; Gu, P.; Yan, Z.; Tang, C.; Xu, Z.; Liu, B.; Liu, Z. Electrically modulating and switching infrared absorption of monolayer graphene in metamaterials. *Carbon* **2020**, *162*, 187–194. [[CrossRef](#)]
100. Qing, Y.M.; Ma, H.F.; Ren, Y.Z.; Yu, S.; Cui, T.J. Near-infrared absorption-induced switching effect via guided mode resonances in a graphene-based metamaterial. *Opt. Express* **2019**, *27*, 5253–5263. [[CrossRef](#)]
101. Liu, Z.; Zhou, J.; Liu, X.; Fu, G.; Liu, G.; Tang, C.; Chen, J. High-Q plasmonic graphene absorbers for electrical switching and optical detection. *Carbon* **2020**, *166*, 256–264. [[CrossRef](#)]
102. Liu, J.; Tang, S.; Ren, B.; Song, J.; Jiang, Y. Tunable ultra-high quality factor graphene absorber based on semicylindrical silica array and distributed Bragg reflector structure. *AIP Adv.* **2022**, *12*, 055125. [[CrossRef](#)]
103. Zhong, H.; Liu, Z.; Liu, X.; Fu, G.; Liu, G.; Chen, J.; Tang, C. Ultra-high quality graphene perfect absorbers for high performance switching manipulation. *Opt. Express* **2020**, *28*, 37294–37306. [[CrossRef](#)]
104. Wan, S.; Qin, C.; Wang, K.; Li, Y.; Guan, C.; Lv, B.; Li, W.; Shi, J. Ultra-high quality perfect absorber based on quasi bound states in the continuum. *J. Appl. Phys.* **2022**, *131*, 213104. [[CrossRef](#)]
105. Zhu, J.; Yin, J.; Wu, C. Tunable Perfect Absorber of Graphene Metamaterial in the Terahertz Band and Its Sensing Properties. *Adv. Photonics Res.* **2022**, *3*, 2100291. [[CrossRef](#)]
106. Yan, Z.D.; Zhu, Q.; Wan, M.J.; Lu, X.; Pu, X.T.; Tang, C.J.; Yu, L.L. Graphene ultraviolet ultrahigh-Q perfect absorption for nanoscale optical sensing. *Opt. Express* **2020**, *28*, 6095–6101. [[CrossRef](#)]
107. Nematpour, A.; Lisi, N.; Lancellotti, L.; Chierchia, R.; Grilli, M.L. Experimental Mid-Infrared Absorption (84%) of Single-Layer Graphene in a Reflective Asymmetric Fabry–Perot Filter: Implications for Photodetectors. *ACS Appl. Nano Mater.* **2021**, *4*, 1495–1502. [[CrossRef](#)]
108. Huang, C.H.; Wu, C.H.; Bikbaev, R.G.; Ye, M.J.; Chen, C.W.; Wang, T.J.; Timofeev, I.V.; Lee, W.; Chen, K.P. Wavelength- and Angle-Selective Photodetectors Enabled by Graphene Hot Electrons with Tamm Plasmon Polaritons. *Nanomaterials* **2023**, *13*, 693. [[CrossRef](#)]
109. Lee, I.H.; Yoo, D.; Avouris, P.; Low, T.; Oh, S.H. Graphene acoustic plasmon resonator for ultrasensitive infrared spectroscopy. *Nat. Nanotechnol.* **2019**, *14*, 313–319. [[CrossRef](#)]
110. Wang, M.; Xiao, Y.; Li, Y.; Han, L.; Sun, Z.; He, L.; Liu, R.; Hu, K. Recent Progress on Graphene Flexible Photodetectors. *Materials* **2022**, *15*, 4820. [[CrossRef](#)]
111. Marchena, M.; Wagner, F.; Arluguie, T.; Zhu, B.; Johnson, B.; Fernández, M.; Chen, T.L.; Chang, T.; Lee, R.; Pruneri, V. Dry transfer of graphene to dielectrics and flexible substrates using polyimide as a transparent and stable intermediate layer. *2D Mater.* **2018**, *5*, 035022. [[CrossRef](#)]
112. Lu, W.B.; Wang, J.W.; Zhang, J.; Liu, Z.G.; Chen, H.; Song, W.J.; Jiang, Z.H. Flexible and optically transparent microwave absorber with wide bandwidth based on graphene. *Carbon* **2019**, *152*, 70–76. [[CrossRef](#)]

Disclaimer/Publisher’s Note: The statements, opinions and data contained in all publications are solely those of the individual author(s) and contributor(s) and not of MDPI and/or the editor(s). MDPI and/or the editor(s) disclaim responsibility for any injury to people or property resulting from any ideas, methods, instructions or products referred to in the content.